THE JOURNAL OF BIOLOGICAL CHEMISTRY
Vol. 278, No. 27, Issue of July 4, pp. 24680–24687, 2003
Printed in U.S.A.

Crystal Structure of Varicella Zoster Virus Thymidine Kinase*

Received for publication, February 26, 2003, and in revised form, April 8, 2003
Published, JBC Papers in Press, April 9, 2003, DOI 10.1074/jbc.M302025200

Louise E. Bird‡§, Jingshan Ren‡§, Alan Wright‡, Kris D. Leslie‡, Bart Degrève¶, Jan Balzarini¶, and David K. Stammers‡‖

From the ‡Division of Structural Biology, The Wellcome Trust Centre for Human Genetics, Henry Wellcome Building of Genomic Medicine, University of Oxford, Roosevelt Drive, Headington, Oxford, OX3 7BN, United Kingdom and ¶Rega Institute for Medical Research, Katholieke Universiteit Leuven, B-3000 Leuven, Belgium

Herpes virus thymidine kinases are responsible for the activation of nucleoside antiviral drugs including (*E*)-5-(2-bromovinyl)-2′-deoxyuridine. Such viral thymidine kinases (tk), beside having a broader substrate specificity compared with host cell enzymes, also show significant variation in nucleoside phosphorylation among themselves. We have determined the crystal structure of Varicella zoster virus (VZV, human herpes virus 3) thymidine kinase complexed with (*E*)-5-(2-bromovinyl)-2′-deoxyuridine 5′-monophosphate and ADP. Differences in the conformation of a loop region (residues 55–61) and the position of two α-helices at the subunit interface of VZV-tk compared with the herpes simplex virus type 1 (human herpes virus 1) enzyme give rise to changes in the positioning of residues such as tyrosine 66 and glutamine 90, which hydrogen bond to the substrate in the active site. Such changes in combination with the substitution in VZV-tk of two phenylalanine residues (in place of a tyrosine and methionine), which sandwich the substrate pyrimidine ring, cause an alteration in the positioning of the base. The interaction of the (*E*)-5-(2-bromovinyl)-2′-deoxyuridine deoxyribose ring with the protein is altered by substitution of tyrosine 21 and phenylalanine 139 (analagous to herpes simplex virus type 1 histidine 58 and tyrosine 172), which may explain some of the differences in nucleoside sugar selectivity between both enzymes. The altered active site architecture may also account for the differences in the substrate activity of ganciclovir for the two thymidine kinases. These data should be of use in the design of novel antiherpes and antitumor drugs.

Varicella zoster virus (VZV[1]; human herpes virus 3) is the causative agent for both a primary (chicken pox or Varicella) and a secondary disease (shingles or zoster), the latter results from activation of the latent virus. Whereas Varicella is generally considered to be a mild childhood disease, in adults it may be complicated by pneumonia and encephalitis and in immunocompromised patients it is associated with significant morbidity and mortality (1).

The mammalian thymidine kinase is part of the pyrimidine salvage pathway and catalyzes the transfer of the γ-phosphoryl group from ATP to thymidine to give thymidine monophosphate. Both HSV1-tk (human herpes virus 1-tk) and VZV-tk have an additional thymidylate kinase activity that converts thymidine monophosphate to thymidine diphosphate. The substrate specificity of VZV-tk is also broader than the host cell kinase with a wide range of nucleoside analogues able to be phosphorylated (2–4). Many of the drugs utilized to treat herpes virus infections are nucleoside analogues such as the pyrimidine nucleoside BVDU or the guanine nucleoside analogues, aciclovir and ganciclovir (Scheme 1), which are activated by the viral thymidine kinase (4).

Thus, the broad substrate specificity of herpes virus thymidine kinases is of interest pharmaceutically, both for the action of antiviral drugs and increasingly for their potential use in enzyme pro-drug gene therapy of tumors (5–7). In both cases, cells expressing the viral thymidine kinase either monophosphorylate or diphosphorylate nucleoside analogues. Further metabolism by cellular enzymes results in the formation of nucleotide triphosphates that either inhibit cellular DNA polymerases by substrate competition (*e.g.* idoxuridine) or by DNA chain termination (*e.g.* ACV), thereby causing cell death (4).

The HSV1 and HSV2 thymidine kinases (human herpes virus 1 and 2, respectively) have 79% amino acid sequence identity, whereas VZV-tk is more divergent, sharing only 29% overall sequence identity with either of the herpes simplex virus enzymes (8). When considering the nucleoside selectivity of VZV both for a series of related compounds against VZV-tk and a comparison with the specificity of HSV1-tk, a number of differences have been determined (3, 9–13). However, care must be taken in interpreting nucleoside specificity results because data for many compounds have only been derived from antiviral assays in tissue culture, which thus means that in any comparison a series of steps are being assessed. Thus, in addition to the DNA polymerase, a series of nucleoside activation steps (including the thymidine kinase) are being assayed. Studies have shown while enzyme and antiviral assays may correlate for some 5-substituted uracil nucleoside analogues as well as the purine analogues ACV and GCV, it is not the case for all of the nucleosides (14, 15). For example, the EC_{50} for ethyl-DU, vinyl-DU, ethynyl-DU, propynyl-DU, and bromovinyl-DU against VZV-infected cells were found to be >12,000-fold different. However, the K_i values determined for the nucleosides against VZV-tk in the same study show only a 20-fold difference, indicating that a relatively minor component

* This work was supported in part by the "Belgische Federatie tegen kanker" (to J. B.), the Medical Research Council (to D. K. S.), and the European Commission Grant QLG1-CT-2001-01004 (to J. B. and D. K. S.). The costs of publication of this article were defrayed in part by the payment of page charges. This article must therefore be hereby marked "*advertisement*" in accordance with 18 U.S.C. Section 1734 solely to indicate this fact.

The atomic coordinates and structure factors (code 1OSN) have been deposited in the Protein Data Bank, Research Collaboratory for Structural Bioinformatics, Rutgers University, New Brunswick, NJ (http://www.rcsb.org/).

‖ To whom correspondence should be addressed. Tel.: 44-1865-287565; Fax: 44-1865-287547; E-mail: Daves@strubi.ox.ac.uk.

§ Both authors contributed equally to this work.

[1] The abbreviations used are: VZV, Varicella zoster virus; ACV, aciclovir; BCNA, bicyclic pyrimidine nucleoside analogue; BVDU, (*E*)-5-(2-bromovinyl)-2′-deoxyuridine; BVDU-MP, (*E*)-5-(2-bromovinyl)-2′-deoxyuridine 5′-monophosphate; DU, deoxyuridine; GCV, ganciclovir; HSV, herpes simplex virus (human herpes virus); tk, thymidine kinase; r.m.s., root mean square; GST, glutathione *S*-transferase; NCS, noncrystallographic symmetries; BVaraU, (*E*)-5-(2- bromovinyl)-1-β-D-arabinofuranosyluracil.

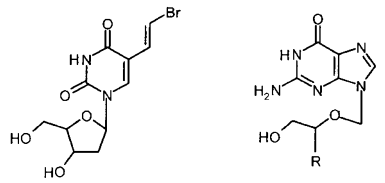

SCHEME 1. **Acyclic purine nucleosides: ACV, R = H; GCV, R = CH_2OH.**

of this selectivity is attributable to the tk activation step. ACV has been the main drug of choice against VZV and HSV infections (16), although its antiviral activity is much greater against HSV (types 1 and 2) than it is against VZV (4, 17), a result of the differing affinities for the thymidine kinases where the K_i for ACV against VZV-tk is 830 μM (18) compared with 200 μM for HSV1-tk (19, 20). Even more marked is the difference in potency for GCV, which binds with a similar affinity to VZV-tk as ACV but more tightly to HSV1-tk with a K_i of 48 μM (7, 21).

BVDU (brivudin) has been licensed for the treatment of VZV in Germany and is undergoing licensing approval in a number of other European countries (4). The efficacy of BVDU is similar for both HSV1 and VZV. Both tks have K_i values of 0.1 μM and similar k_{cat}/K_m values (15, 19, 22). The most potent compounds against VZV are found within the BVDU-related halogen-vinyl araU series. For example, the EC_{50} for BVaraU (sorivudine) against VZV is 0.0023 μM with chlorovinyl- and iodovinyl-araU having similar values (15). BVDU is 19-fold less potent against the virus than BVaraU; however, the K_i values against VZV-tk are 0.25 and 0.1 μM, respectively, suggesting that most of the difference in selectivity for VZV-infected cells is not the result of the thymidine kinase (15). The EC_{50} for BVaraU against HSV1 is 0.06 μM compared with 0.0023 μM for VZV (15). A chimeric HSV1 constructed to express the VZV-tk instead of HSV1-tk had the same sensitivity to BVaraU as VZV, suggesting that in this case the increased potency of this compound is attributable to the thymidine kinase (14). VZV-tk shows some selectivity for the sugar moiety of nucleoside analogues. The K_i values for 2-deoxyribose, arabinose, 2-fluoroarabinose, and ribose derivatives of BV-uracil nucleosides are 0.12, 0.25, 2.75, and 4.48 μM, respectively (15).

Although there have been several reports of the crystal structure determination of HSV1-tk complexes (23–26), there have been no other herpes thymidine kinase structures published as yet. To investigate the basis of differences in substrate specificity of herpes virus thymidine kinases, we have solved the crystal structure of VZV-tk complexed with BVDU-MP and ADP. This structure will both aid the rational design of novel ligands for use as drugs to treat viral infections as well as for combined gene therapy/chemotherapy approaches to provide a novel means of treating cancer.

EXPERIMENTAL PROCEDURES

Cloning, Expression, and Purification—A pGEX-5X-1 (Amersham Biosciences) derived construct with the entire VZV-tk coding sequence contained in a *Eco*RI/*Sal*I fragment was used as the source of the VZV-tk gene.[2] The gene was transferred as a *Eco*RI/*Sal*I fragment into pGEX-6P-1 (Amersham Biosciences) to make the expression vector pGEX6P1VZV-TK, which has a rhinovirus 3C protease cleavage site (utilized to remove the GST). The expression plasmid was transformed into BL21 for protein expression. 5 μl of the transformation mixture was used to inoculate 120 ml of LB + 50 μg/ml carbenicillin, and the culture was grown overnight with shaking at 37 °C. The culture was then diluted 1/50 into 6 liters and grown at 37 °C until the A_{600} reached 0.5. Isopropyl-1-thio-β-D-galactopyranoside was added to 0.1 mM, and induction was carried out at 18 °C for 18 h. The cells were harvested by centrifugation, and the cell pellet was frozen at −80 °C until required. After defrosting, the cell pellet was resuspended in buffer A (50 mM Tris, pH 7.4, 5 mM EDTA, 1% (v/v) Triton X-100). Lysozyme was added to the cell suspension to a final concentration of 40 μg/ml, and it was stirred for 20 min at room temperature prior to being sonicated on ice and then stirred further at room temperature for 30 min. The supernatant was clarified by centrifugation and applied at 0.25 ml/min to a 5-ml glutathione-Sepharose column (GST-Trap, Amersham Biosciences) pre-equilibrated with buffer A. The column was washed with buffer A until the base line returned to zero followed by buffer B (50 mM Tris, pH 7.4, 150 mM NaCl, 1 mM dithiothreitol, 1 mM EDTA) until the base line restabilized. 0.5 mg of GST-3C protease was added to the column in 5 ml of buffer B, and the column was incubated overnight at 4 °C. The VZV-tk was eluted at 0.2 ml/min by washing the GST column with buffer B, the outlet flow was directed through a 1-ml GST-Trap column connected in series (this is to help bind any free GST, GST-3C, and GST-VZV-tk). The pool from the GST-Trap column was concentrated by centrifugation in Vivaspin 6 concentrators (Vivascience) and applied to a Superdex 200 HR gel filtration column pre-equilibrated with buffer C (100 mM Tris, pH 7.4, 200 mM NaCl). The fractions containing the VZV-tk were pooled, diluted 4-fold with water to give a buffer concentration of 25 mM Tris, pH 7.4, and 50 mM NaCl, concentrated to 8 mg/ml by centrifugation in Vivaspin 2 concentrators, and stored frozen at −80 °C.

Crystallization, Data Collection, and Structure Solution—Screening for crystallization conditions was carried out using a variety of commercially available screening kits (Hampton Research) together with a range of ligand sets. Thin plate-like crystals were obtained using a sitting drop vapor-diffusion method by mixing 1 μl of protein and 1 μl of reservoir solution at 21 °C. Despite screening a large range of ligand combinations, crystals were only obtained from 8 mg/ml VZV-tk with the addition of 0.4 mM ATP, 0.2 mM BVDU, and 0.6 mM $MgCl_2$ (these conditions were intended to give the products of the thymidylate kinase reaction) and reservoirs containing 100 mM sodium acetate at either pH 4.5 or 5.0 and between 6 and 11% (w/v) polyethylene glycol 20,000.

The x-ray diffraction data were collected at beamline ID14-EH2 at the European Synchrotron Radiation Facility (ESRF). A very thin plate crystal (~10-μm thick) was first soaked in reservoir solution containing 20% glycerol for a few seconds and then flash-frozen and maintained at 100 K during data collection. A total of 360 data frames of 1° oscillation were recorded using an ADSC-Q4 CCD area detector with an exposure time of 12 s/frame and a crystal to detector distance of 250 mm. The data frames were indexed and integrated with DENZO and were merged with SCALEPACK (27). The crystal belongs to the $P2_1$ space group with unit cell dimensions of a = 99.7 Å, b = 54.2 Å, c = 167.8 Å, and β = 94.8°. There are four subunits in the asymmetric unit and a crystal solvent content of 58%. The final data set is 99.9% complete to a 3.2-Å resolution with a merging R-factor of 0.171 and a redundancy of >5-fold (Table I).

The structure of VZV-tk was determined by molecular replacement. The self-rotation function revealed two 2-fold non-crystallographic symmetries (NCS), one parallel to the crystal 2-fold screw axis and another on the XZ plane. Real space cross-rotation function, PC refinement of the rotation peaks, and fast F2F2 translation searches with CNS (28) using the HSV1-tk dimer (Protein Data Bank accession number 1E2K (see Ref. 29)) as the search model resulted in the correct orientations and positions of the two VZV-tk dimers in the crystal asymmetric unit. The two monomers of each dimer are related by a 2-fold NCS, and the two dimers are related by a rotation of 165°.

Given the relatively low sequence identity (29%) between VZV and HSV-1 tks, unsurprisingly, the initial R-factor (50.2%) for data between 10.0- and 4.0-Å resolution was high. Although the x-ray data are relatively weak and only to a moderate resolution, the refinement of VZV-tk structure greatly benefited from the use of 4-fold NCS restraints. The model rebuilding has been made possible by 4-fold NCS real space electron density averaging using the program GAP.[3]

Modeling of Ganciclovir Binding to VZV-tk—The docking of GCV was carried out using G.O.L.D., version 1.2, with the genetic algorithm set at "default parameter settings." An appropriate center point for each docking run was chosen with a calculation radius of 20 Å on chain A of VZV-tk. Additional fitness flags included the flipping of free corners, planar nitrogens, and amide bonds, and a total of 20 dockings were set up for each ligand run with a r.m.s. tolerance of 1.5 Å for early termination. Once docking was complete, the top three solutions were subjected to conjugate gradient minimization using the program NAMD2

[2] J. Balzarini and B. Degrève, unpublished data.

[3] D. I. Stuart, J. M. Grimes, and J. M. Diprose, unpublished program.

TABLE I
Statistics for crystallographic structure determination

Data collection details	
Data collection site	ESRF 1D14-EH2
Detector	CCD ADSC-Q4
Wavelength (Å)	0.933
Space group	$P2_1$
Unit cell dimensions (a, b, c in Å)	99.7, 54.2, 167.8, β = 94.8°
Resolution range (Å)	30.0-3.20
Observations	167134
Unique reflections	30040
Completeness (%)	99.9
Average I/σ(I)	4.5
R_{merge}	0.171
Outer resolution shell	
Resolution range (Å)	3.31-3.20
Unique reflections	2925
Completeness (%)	99.6
Average I/σ(I)	1.1
Refinement statistics	
Resolution range (Å)	30.0-3.20
No. of reflections (working/test)	28537/1490
R-factor (R_{work}/R_{free})	0.236/0.267
No. atoms (protein/substrate-inhibitor)	9914/200
R.m.s. bond-length deviation (Å)	0.0086
R.m.s. bond-angle deviation (°)	1.32
Mean B-factor (Å^2)	36/40/77
R.m.s. backbone B-factor deviation (Å^2)	4.5

and the CHARMM22 force-field. For this, an 8-Å radius was defined from the center point of each docked ligand where full flexibility was imparted to the surrounding protein structure. Atoms beyond this radius were fixed during the calculation to maintain the overall integrity of the crystal structure.

RESULTS

Overall Structure—The final refined structure (Protein Data Bank accession number 1OSN) has an $R_{working}$ of 0.236 and an R_{free} of 0.267 for all of the data to 3.2-Å resolution with retention of excellent stereochemistry. The r.m.s. deviations from ideality for the model are 0.0086 Å for bond lengths and 1.3° for bond angles (Table I). Because of the tight NCS restraints in the refinement, the r.m.s. deviation for Cα atoms between any two monomers is <0.1 Å. The current VZV-tk model has electron density present for residues: 8–185 and 192–338 in the A chain (for residues 185 and 192–194, density is only visible for the main chain) and 8–112, 124–185, and 195–338 in the B, C, and D chains, respectively. In addition, there are four BVDU-MP and four ADP ligands. The quality of the electron density is exemplified by the maps shown in Fig. 1, *a* and *b*. The original GenBank™ entry for VZV-tk available at the time that we started the structure determination had residue 143 annotated as a glycine, whereas in common with HSV1 and HSV2-tk sequences (Fig. 2), the electron density clearly shows an arginine (Fig. 1*a*). Sequencing of the plasmid and subsequent updates of GenBank™ have confirmed this assignment. The two dimers in the asymmetric unit of the crystal are cross-linked by a disulfide bridge between the Cys-63 residues on the A and D subunits (Fig. 1*c*). However, given its intracellular location and the lack of evidence that VZV-tk or indeed any other herpes virus thymidine kinases function as tetramers, it is likely that this cross-linking it not biologically relevant and occurred during the crystallization process.

Despite the relatively low degree of overall amino acid sequence identity (29%) with both the herpes simplex enzymes (8), 258 of 325 Cα atoms from VZV-tk superimpose onto HSV1-tk (Protein Data Bank accession number 1E2K) with an overall r.m.s. deviation of 1.3 Å. Thus, there is a general structural similarity with both HSV1-tk and the related adenylate kinase structure (23, 24, 30, 31) (Fig. 1*d*). However, there are some differences. The loop between residues 110 and 122 in VZV-tk is longer than the equivalent loop in HSV1-tk (residues 145–154) because of an insertion of two residues (Figs. 1*d* and 2), and in contrast to HSV1-tk structures, residues 231–249 are ordered with amino acids 232–241, forming a short α-helix. The two monomers in the VZV-tk dimer are related by 2-fold symmetry; however, the orientation of the symmetry axis is different from HSV1-tk such that if the A chains of HSV1-tk and VZV-tk are overlapped, there is a 9° offset between the B chains. The dimerization interface in HSV1-tk chiefly consists of residues from five helices (Fig. 2, *α2*, *α4*, *α5*, *η2/α8*, and *α13* in VZV-tk), the C terminus, and a loop (23, 24). The majority of the interface in VZV-tk comprises the same secondary structural elements as HSV1-tk; however, the nature of the side chains involved is quite different. An alignment of the HSV1-tk structure to the core secondary structure elements containing the active site (Protein Data Bank accession number 1KI8 (see Ref. 26)) shows that although the Cα backbone of most of the molecule aligns well, residues 55–95 do not (Figs. 1*d* and 3*a*). This is the result of two major structural differences in the subunit interface and active site structural elements, namely in residues 51–54 (helix α2), the loop between amino acids 55 and 61 (HSV1-tk-(90–96)) and in the helices and loops comprising residues 62–106 (Fig. 3*a*, α3, α4, and α5 in HSV1-tk-(112–141)). In the subunit interface, to accommodate Trp-277 (HSV1-tk Phe-308) on the one subunit, there is a conformational change within the loop (residues 55–61) relative to HSV1-tk. The loop conformation is stabilized by hydrogen bonding between Glu-59 with His-8 (both from the A chain) and Arg-84 from the B chain. The loop movement relative to HSV1-tk results in the conserved amino acids Tyr-52 (in the preceding α2 helix; HSV1-tk-87) and Leu-56 (in the loop; HSV1-tk-91) having completely different conformations and interactions across the subunit interface (Fig. 3*a*). Following the loop, amino acids in the α3 and α4 helices that contain both active site residues such as Tyr-66 and Gln-95 and make subunit interface contacts have differences between 1.0 and 4.4 Å in Cα positions for the two tks.

Structural Analysis of the Active Site—Despite low overall amino acid sequence identity, there is locally higher identity in six conserved regions found in all of the herpes virus thymidine kinases (8, 32–34). Many of these sequences constitute the active site, which can be viewed as comprising the ATP and the thymidine binding pockets, respectively. These are discussed in detail below.

ADP Binding Site—ADP is observed in the VZV-tk structure reported indicating that a product complex had been crystallized (Figs. 1*b* and 3*b*). The interactions of ADP with the enzyme are similar to those for HSV1-tk (25). Arg-183 and Pro-302 (HSV1-tk Arg-216 and Pro-333, respectively) sandwich the adenine base, and the main chain carbonyl of Gln-300 (HSV1 Gln-331) hydrogen bonds to N-6 while Thr-27 (HSV1-tk Thr-64) makes a weak hydrogen bond to the N-7 atom of the adenine ring. Residues 22–27 form the phosphate binding site of VZV-tk (the P loop) with a network of hydrogen bonds to the α- and β-phosphates of ATP, comparable with that observed in HSV1-tk for residues 59–64 (25). Asp-162 in HSV1-tk is proposed to coordinate magnesium, and the corresponding Asp-129 in VZV-tk is in the same position consistent with this hypothesis (23). The polypeptide chain between amino acids 184 and 193 in VZV-tk is largely disordered, whereas the equivalent region in HSV1-tk (residues 212–226) forms part of a lysine/arginine-rich loop known as the flap or "lid" that encloses the ATP site and makes contacts with the phosphates (25, 26). The lid region has been shown to be flexible in HSV1-tk and adenylate kinase, being able to adopt open and closed conformations (21). The disordering of the VZV-tk lid is

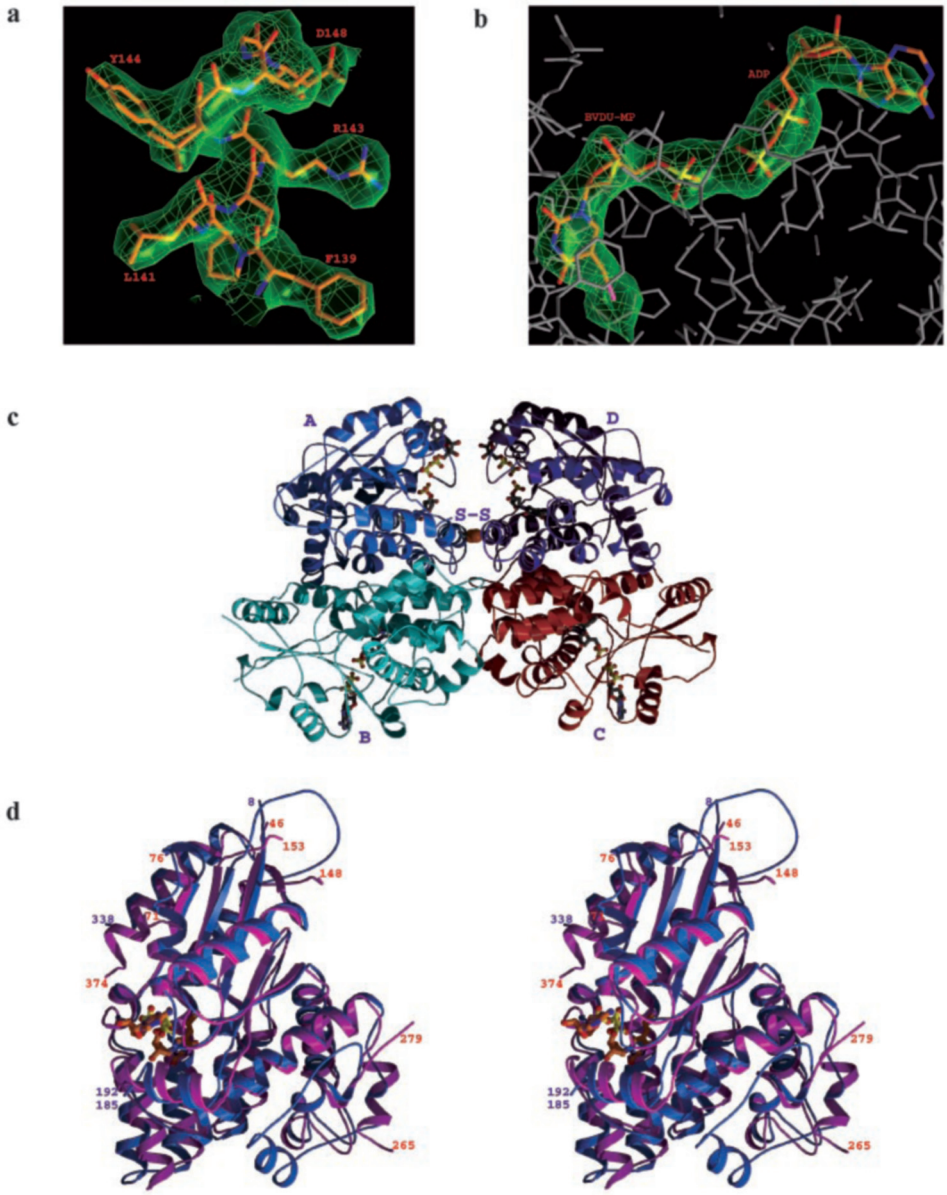

FIG. 1. **Overall structure of VZV-tk.** *a*, a representative $2F_o - F_c$ electron density map contoured at 1σ showing residues 139–148 of the A subunit. *b*, simulated-annealing omit electron density map contoured at 3σ showing the bound BVDU-MP and ADP in the A subunit. *c*, the two dimers in the crystal asymmetric unit. Protein chains are shown as *ribbons* and *coils*, and each monomer is *colored* differently. The bound BVDU-MPs and ADPs are shown as *ball-and-sticks*. The disulfide bridge between the two dimers is indicated by two *orange spheres*. *d*, Stereodiagram showing VZV-tk (*blue*) overlapped with HSV1-tk (*magenta*). Residue *numbers* at chain breaks are *labeled*.

consistent with the presence of the product or open complex where the release of ADP can be facilitated following catalysis.

Pyrimidine Binding Site—In the pyrimidine binding site, BVDU-MP is present, consistent with a single turnover of the enzyme having occurred (Figs. 1*b* and 3*b*). By analogy with HSV1-tk, there are two pockets named P1 and P2, which recognize the base and sugar (-like) moieties, respectively (35). The P1 region contains an additional subpocket that contacts 5-substituent on the pyrimidine ring. A detailed examination of these pockets in VZV-tk reveals both similarities and differences with HSV1-tk. In P1, there are two hydrogen bonds to Gln-90 (HSV1-tk Gln-125) from the pyrimidine N-3 and O-4, which orientates the base, whereas the differing loop conformation discussed above results in the Cα position of Gln-90 and HSV1-tk Gln-125 being 2.3 Å apart. Nevertheless, the Cγ atom of the respective Gln side chains are positioned within 0.4 Å of each other, resulting in a similar pattern of hydrogen bonds. Arg-176 in HSV1-tk interacts with the pyrimidine base via two ordered water molecules. The equivalent residue in VZV-tk, Arg-43, is in a similar position, and there is enough space to accommodate two water molecules in the vicinity. Indeed, there is evidence in the electron density map for one of these waters. Therefore, it seems likely that water-mediated hydrogen bonding will be conserved in the two enzymes. In VZV-tk, the pyrimidine ring of BVDU is stacked between two aromatic residues, Phe-93 and Phe-139, with additional van der Waals contacts made with Ile-62 (Fig. 3*b*). This is in marked contrast to HSV1-tk where the base is sandwiched by an aliphatic and aromatic residue, Met-128 and Tyr-172, respectively, with Ile-100 also making some contacts (19, 26, 36). These differences in interactions with the pyrimidine ring result in the base binding in a significantly different position to that seen in the HSV1-tk structure. Although the average atom displacement between the BVDU molecules in the two structures is 0.9 Å, the C-4 and C-5 atoms show the best overlap (0.3 Å apart), the C-2 and N-1 atoms are displaced by 0.6 and 0.7 Å, respectively, and the

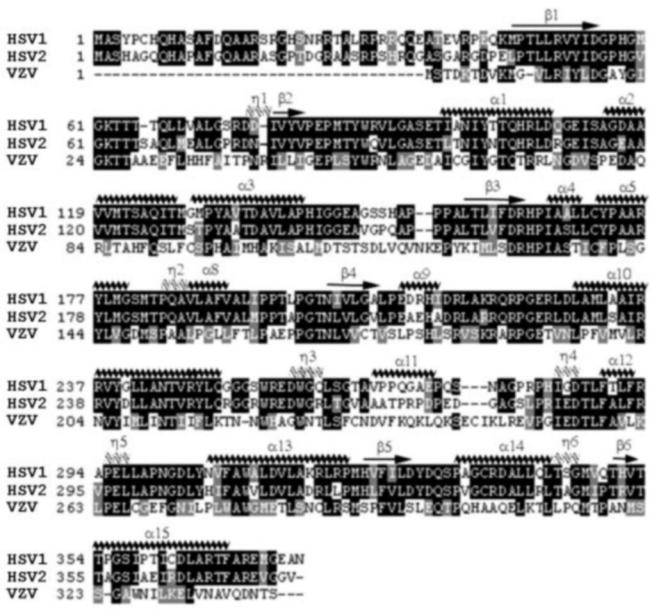

FIG. 2. **Sequence alignment of VZV-tk with HSV1 and HSV2 tks.** *Filled residues* indicate amino acid identity, and *shaded residues* indicate similarity. The VZV-tk secondary structure (assigned by Dictionary of secondary structure of proteins) is shown above the alignment. α, β, η, and ***T*** indicate an α-helix, β-strand, 3^{10} helix, and hydrogen-bonded turn, respectively.

ribose C-5 is the greatest displacement at 1.6 Å apart. The plane of the BVDU pyrimidine ring in VZV-tk is displaced by an angle of ~14° compared with that of HSV1-tk (Fig. 3*c*). The 5-bromovinyl substituent of BVDU in VZV-tk makes van der Waals contacts in a subpocket with Trp-53, His-97, Arg-130, Ala-134, and Ser-135. In HSV1-tk, the substitution of tyrosine 132 for His-97 and alanine 168 for Ser-135 results in a change in subpocket shape and also hydrogen-bonding potential. Despite the overall similarities of the residues that interact with the 5-bromovinyl substituent, the BVDU bromine atom is 0.7 Å from the position in HSV1-tk (Fig. 3*c*), altering its interaction with VZV-tk compared with HSV1-tk. Thus, His-97 is more closely associated with the bromine than Tyr-132 (HSV1-tk). Additionally, Ser-135 makes more and closer van der Waals contacts than Ala-168 (HSV1-tk). The backbone nitrogen of Ser-135 is 3.7 Å from the bromine atom in VZV-tk, whereas for HSV1-tk, the equivalent nitrogen (Ala-168) to bromine atom distance is 4.3 Å.

The sugar moiety of BVDU-MP binds in pocket P2 (Fig. 3*b*), and although it lies in a similar plane to that seen in the HSV1-tk structure, its atoms are displaced by between 1.1 and 1.6 Å compared with the latter case. Such a shift is the result of the difference in the positioning of the pyrimidine ring in the two structures. There is one hydrogen bond between Tyr-66 and the deoxyribose 3′-hydroxyl, an interaction that is conserved in VZV-tk and HSV1-tk (Fig. 3*c*). The remaining interactions involve van der Waals contacts with residues Trp-53 (HSV1-tk Trp-88), Ile-62 (Ile-97), Phe-93 (Met-128), and Phe-139 (Tyr-172). Equivalent contacts are also present in the HSV1-tk product complex. Additional van der Waals interactions are seen for HSV1-tk and the BVDU deoxyribose involving His-58 (Tyr-21) with the C-2 and C-3 atoms and Arg-222 with the C-4 and C-5 atoms (Fig. 3*c*). Arg-186, the VZV-tk equivalent of Arg-222, is in the lid and is disordered in our structure; however, its conservation among a range of herpes tks suggests that an equivalent interaction to that seen in HSV1-tk may be present in the closed complex. Tyr-21 in VZV-tk is structurally equivalent to His-58 (HSV1-tk) but only makes weak van der Waals (>4 Å) interactions with the deoxyribose of BVDU. This seems to be a result of the pyrimidine binding mode where the difference in deoxyribose position is not fully compensated for by a change in the side chain position of Tyr-21. As would be expected, Tyr-21 has a completely different hydrogen-bonding pattern within the VZV-tk active site compared with His-58 (HSV1-tk), making a single interaction with the carbonyl of Ala-193, whereas His-58 hydrogen bonds to Tyr-101 (Tyr-66) and Tyr-172 (Phe-139), residues important for ribose 3′-hydroxyl and pyrimidine binding, respectively.

Enzyme kinetic data indicate that a range of 5-substituted-DUs (ethyl-DU, vinyl-DU, bromovinyl-DU, and ethynyl-DU) can act as substrates for VZV-tk with variations in the affinity of ~20-fold (15). An examination of the VZV-tk model shows that all of these 5-substituents on the pyrimidine ring can be accommodated, although differences in geometries and bulk mean variation in contact with residues lining the subpocket. The compound with the bromovinyl substituent has the lowest K_i value and as described above makes the most extensive contacts within the pocket. Other 5-substituents, with the exception of the 5-propynyl-DU, would make less contact because of lower bulk. The interaction with Trp-53 of the vinyl and ethyl substituents appears more optimal than for ethynyl-DU and propynyl-DU on account of the geometry of the 5-substituent. For 5-propynyl-DU, which has the lowest affinity in this series, the linear carbon-carbon triple bond means that the terminal methyl group is approximately 1.4 Å from the bromine atom position of BVDU, resulting in an unfavorably close interaction among the methyl group and Arg-130 and Ala-134. Data for BVaraU indicate that this nucleoside has different affinities for VZV-tk and HSV1-tk of ~20-fold (14, 15). Inspection of the VZV-tk and HSV1-tk models indicates that the arabinofuranosyl sugar shows differences in the interaction of the 2′-hydroxyl with the respective proteins. In VZV-tk, it can apparently make van der Waals interactions with Phe-139 and Tyr-21, whereas in HSV1-tk, the 2′-hydroxyl makes a van der Waals interaction with His-58 and a close contact with Tyr-172.

Modeling Ganciclovir into VZV-tk—Because we can only obtain crystals in the presence of ATP and BVDU, we have modeled GCV into the active site to understand the binding of purine substrates. Docking of GCV was carried out using the program G.O.L.D. (37) followed by energy minimization with NAMD2 (38). GCV appears unable to bind in exactly the same position as in HSV1-tk because of a steric clash with Phe-139 (Fig. 4*a*). Moreover, Gln-90, which has a different position relative to HSV1-tk Gln-125, would not be able to hydrogen bond in the same orientation as in the HSV1-tk structure, suggesting that in VZV-tk the guanine base may bind in the same plane as the thymidine base. The minimization predicted two energetically very similar binding modes related by a rotation of ~180° about the C-3=C-4 bond of the purine ring. However, in only one of the binding modes was the 4′-hydroxyl as defined by Brown *et al.* (23) in a position to be phosphorylated. In this mode, the purine ring is sandwiched between Phe-93 and Phe-139 and makes two hydrogen bonds to Gln-90, which is in the same position as the BVDU-bound structure, and there is a 1.1-Å difference in the position of the BVDU 5′-hydroxyl and the equivalent (4′-hydroxyl) of GCV.

DISCUSSION

The determination of the crystal structure of VZV-tk revealed the presence of BVDU-MP and ADP, indicating that a single enzyme turnover had occurred, forming a product complex. Although the diffraction of VZV-tk crystals is limited to 3.2 Å, nevertheless, the use of four-way averaging has produced a high quality electron density map as demonstrated by the correction of an amino acid sequence error. Structural overlaps suggest that although the VZV and HSV1-tk monomers are

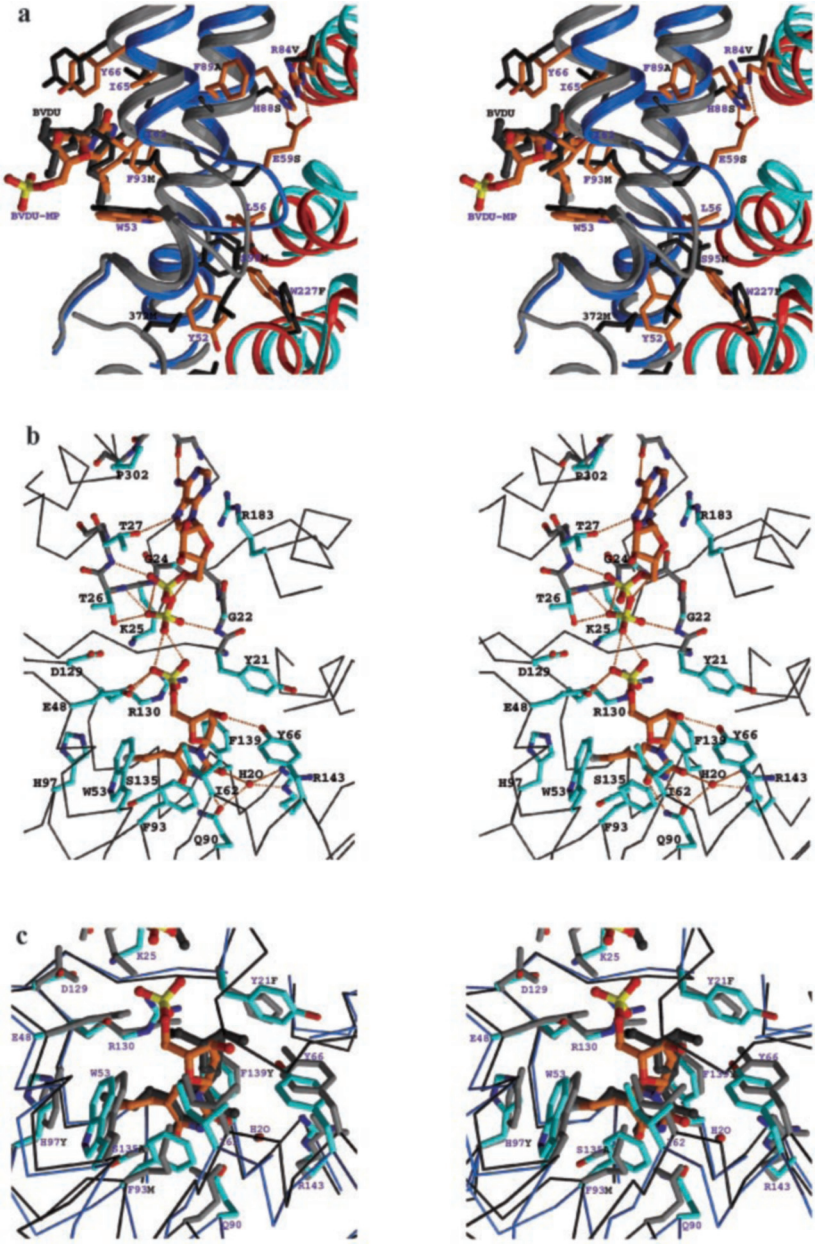

FIG. 3. **The active site structure of VZV-tk.** *a*, stereodiagram showing the difference at the dimer interface between VZV-tk and HSV1-tk and its effect on the active site structure. The main chains are shown as *ribbons* and *coils* with A and B subunits *colored* as *blue* and *cyan* for VZV-tk and *gray* and *red* for HSV1-tk, respectively. The side chains are shown as *sticks* with VZV-tk *colored* in *orange* and HSV1-tk in *dark gray*. If the residue type is different, the last letter in the label indicates the residue name of HSV1-tk. The *orange dotted lines* indicate hydrogen bonds. The BVDU-MP and BVDU associated with VZV-tk and HSV1-tk are shown as *orange* and *dark gray ball-and-sticks*, respectively. *b*, stereodiagram showing the active site of VZV-tk. The Cα backbone is shown as *gray sticks*. The side chains and the bound BVDU-MP and ADP are shown as *ball-and-sticks* and *colored* by atom type with carbon atoms in *cyan* for side chains and *orange* for the substrates. The main chains for residues 21–27 and 300–302 are drawn with carbon atoms in *gray color*. The *orange dotted lines* represent the hydrogen bonds. *c*, the active sites superimposition of VZV-tk and HSV1-tk. The Cα backbone, side chain, and BVDU-MP of VZV-tk are *colored* in *blue*, *cyan*, and *orange*, and those of HSV1-tk are *colored* in *dark gray*, *light gray*, and *black*, respectively.

topologically similar, there are differences including the dimer symmetry axis together with some alteration in secondary structure including an additional helix (α11, amino acids 232–241) as well as an altered loop conformation (residues 55–61) in the dimer interface. Major differences in the conformation of this loop region at the subunit interface (between 1 and 4.4 Å in the Cα position of certain residues) result in some perturbation of the active site. These changes in combination with the differing stacking of the pyrimidine ring between two aromatic phenylalanine residues in VZV-tk compared with methionine/tyrosine side chains in HSV1-tk result in a significant reorientation of the BVDU in the binding site. Interestingly, despite these differences in the modes of interaction the k_{cat}/K_m, parameters for BVDU as a substrate are similar for both VZV and HSV1-tks (15, 19, 22).

The differences in affinity of a range of 5-substituted deoxyuridines reflects alterations in contact with the P1 5-substituent subpocket. The highest affinity is seen for BVDU, which penetrates fully into the pocket, making more extensive contacts. In contrast, the linear carbon-carbon triple bond in 5-propynyl-DU means that although the substituent penetrates the pocket to the same extent as BVDU, its differing position would give a steric clash, explaining its lower affinity. For the other substituents, the extent of the van der Waals contacts with Trp-53 indicates why 5-ethynyl-DU has a lower affinity than either ethyl-DU or vinyl-DU.

Modeling of the arabinofuranosyl sugar into both the VZV-tk and HSV1-tk structures suggests that there are potential differences in the interaction of the 2′-hydroxyl with the respective proteins, particularly the steric clash of the 2′-hydroxyl with Tyr-172. Such an interaction may explain why VZV-tk is able to phosphorylate BV-araU more efficiently than HSV1-tk. There is no obvious structural explanation for the selectivity against the fluoroarabinosyl and fluororibosyl derivatives. A quantum chemical study of the ribose and ribose-like moieties of a series of substrates with HSV1-tk suggest that there is a correlation between the electrical dipole of the sugar-like group and the catalytic activity of the enzyme (35). Thus, it could be that similar effects of conformation and/or polarity are seen with VZV-tk.

A number of long chain fluorescent furano bicyclic pyrimidine analogues (BCNAs) that are monophosphorylated and

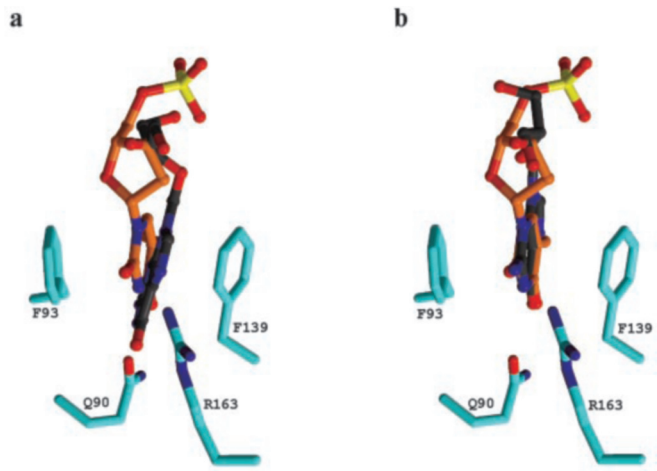

FIG. 4. **Modeling of ganciclovir into the VZV-tk active site.** *a*, overlap of GCV from HSV1-tk with BVDU-MP in the VZV-tk active site. The side chains of VZV-tk are *colored* in *cyan*, and BVDU-MP and GCV are shown as *orange* and *dark gray ball-and-sticks*, respectively. *b*, overlap of BVDU-MP in the VZV-tk active site with modeled GCV. The side chains of VZV-tk are *colored* in *cyan*, and BVDU-MP and GCV are shown as *orange* and *dark gray ball-and-sticks*, respectively.

diphosphorylated by VZV-tk but not HSV-1 tk have been synthesized (22, 39). Modeling into the active site of HSV1-tk based on the nucleoside deoxyribose position suggests that there would be a steric clash with the protein (40). Indeed, it appears that HSV1-tk is unable to bind these analogues because they are not inhibitors of thymidine phosphorylation nor substrates for the enzyme (22, 39, 40). BCNAs cannot be modeled into VZV-tk based on overlaps with the BVDU deoxyribose or base positions without a steric clash with the protein. Therefore, it seems possible that BCNAs might adopt a significantly different binding mode in VZV-tk compared with conventional nucleosides.

The discrimination of HSV1-tk between GCV and ACV is the result of the extra hydrogen bond made between the 3′-hydroxyl equivalent of GCV and His-58 (26). In the HSV1-tk-ACV structure, the absence of the group results in the 5′-hydroxyl binding non-productively in the 3′-hydroxyl position, perhaps explaining the poor activity of this substrate (41). In VZV-tk, Tyr-21 is equivalent to HSV1-tk His-58 and thus cannot make this hydrogen bond, meaning that no difference in affinity of VZV-tk for GCV and ACV would be expected. It is less easy to explain the relative lack of affinity of both ACV and GCV for VZV-tk. Certainly, apart from the interaction with Tyr-21 (HSV1-tk His-58), the conserved nature of the residues in the P2 (deoxyribose binding) site would suggest that the interactions are very similar with the sugar-like moiety. However, the spatial distribution of these residues is different in VZV-tk, therefore suggesting that they may contribute to the low affinity. An analysis of the sequence conservation of ligand-interacting side chains shows there are two residue changes in VZV-tk (namely Met-128 and Tyr-172) to Phe-93 and Phe-139 in VZV-tk, respectively. Interestingly, GCV is a poor substrate for EBV-tk and HHV8-tk, both of which have two phenylalanines at these positions, whereas HSV2-tk, which has the same residues as HSV1-tk, has a similar affinity for ACV (4, 7, 42). Therefore, it seems possible that these residues may also contribute to the low affinity of ACV/GCV for VZV-tk. Docking of GCV and energy minimization confirm that there is room for ACV/GCV to be accommodated in the VZV-tk active site. The docking suggests that GCV may bind with the base in the same plane as that of BVDU in VZV-tk. However, the 4′-hydroxyl is not positioned optimally for phosphorylation to occur. This may explain why GCV and ACV are such poor substrates for VZV-tk. Mutational analysis of HSV1-tk to a VZV-tk-like structure with two phenylalanines completely abolishes catalytic activity with both purine and pyrimidine nucleosides, and these effects can be partially ameliorated by mutating His-58, which interacts with the sugar-like moiety; however, no activity against ACV was observed (20). This again suggests that the orientation of the base, which is a consequence of the difference in active site architecture, affects the positioning of the sugar and hence the catalytic activity. This could explain why guanosine analogues, which have a different sugar-like moiety such as H2G, are more efficacious (7, 42).

The structural data reported here have consequences for the design of nucleoside analogues. It seems likely that the design of guanosine-derived compound that are specific for VZV-tk may be possible but that they will not necessarily have the same structure as HSV1-tk-targeted analogues. The difference in binding of the pyrimidine ring and hence the 5-substituent in its pocket also suggests that further pyrimidine analogues could be designed against VZV-tk. Such nucleoside analogues could have utility as both antiviral agents as well as in applications for cancer therapy using combined gene/chemotherapy approaches.

Acknowledgments—We thank the staff at ESRF (Grenoble, France) for help with the data collection. We also thank Dr. R. Esnouf and J. Dong for computer support.

REFERENCES

1. Snoeck, R., Gerard, M., Sadzot-Delvaux, C., Andrei, G., Balzarini, J., Reymen, D., Ahadi, N., De Bruyn, J. M., Piette, J., Rentier, B., Clumeck, N., and De Clerq, E. (1994) *J. Med. Virol.* **42,** 338–347
2. Fyfe, J. A., Keller, P. M., Furman, P. A., Miller, R. L., and Elion, G. B. (1978) *J. Biol. Chem.* **253,** 8721–8727
3. Fyfe, J. A. (1982) *Mol. Pharmacol.* **21,** 432–437
4. Naesens, L., and De Clercq, E. (2001) *Herpes* **8,** 12–16
5. Grignet-Debrus, C., and Calberg-Bacq, C. M. (1997) *Gene Ther.* **4,** 560–569
6. Degrève, B., Andrei, G., Izquierdo, M., Piette, J., Morin, K., Knaus, E. E., Wiebe, L. I., Basrah, I., Walker, R. T., De Clercq, E., and Balzarini, J. (1997) *Gene Ther.* **4,** 1107–1114
7. De Clercq, E., Naesens, L., De Bolle, L., Schols, D., Zhang, Y., and Neyts, J. (2001) *Rev. Med. Virol.* **11,** 381–395
8. Suzutani, T., Davies, L. C., and Honess, R. W. (1993) *J. Gen. Virol.* **74,** 1011–1016
9. Chen, M. S., and Prusoff, W. H. (1978) *J. Biol. Chem.* **253,** 1325–1327
10. Yokota, T., Konno, K., Mori, S., Shigeta, S., Kumagai, M., Watanabe, Y., and Machida, H. (1989) *Mol. Pharmacol.* **36,** 312–316
11. Suzutani, T., Machida, H., Sakuma, T., and Azuma, M. (1988) *Antimicrob. Agents Chemother.* **32,** 1547–1551
12. Ayisi, N. K., Wall, R. A., Wanklin, R. J., Machida, H., De Clercq, E., and Sacks, S. L. (1987) *Mol. Pharmacol.* **31,** 422–429
13. Cheng, Y. C., Dutschman, G., De Clercq, E., Jones, A. S., Rahim, S. G., Verhelst, G., and Walker, R. T. (1981) *Mol. Pharmacol.* **20,** 230–233
14. Bevilacqua, F., Davis-Poynter, N., Worrallo, J., Gower, D., Collins, P., and Darby, G. (1995) *J. Gen. Virol.* **76,** 1927–1935
15. Ashida, N., Watanabe, Y., Miura, S., Kano, F., Sakata, S., Yamaguchi, T., Suzutani, T., and Machida, H. (1997) *Antiviral. Res.* **35,** 167–175
16. Cohen, J. I., Brunell, P. A., Straus, S. E., and Krause, P. R. (1999) *Ann. Intern. Med.* **130,** 922–932
17. Andrei, G., Snoeck, R., Neyts, J., Sandvold, M. L., Myhren, F., and De Clercq, E. (2000) *Antiviral Res.* **45,** 157–167
18. Roberts, G. B., Fyfe, J. A., Gaillard, R. K., and Short, S. A. (1991) *J. Virol.* **65,** 6407–6413
19. Kussmann-Gerber, S., Kuonen, O., Folkers, G., Pilger, B. D., and Scapozza, L. (1998) *Eur. J. Biochem.* **255,** 472–481
20. Pilger, B. D., Perozzo, R., Alber, F., Wurth, C., Folkers, G., and Scapozza, L. (1999) *J. Biol. Chem.* **274,** 31967–31973
21. Vogt, J., Perozzo, R., Pautsch, A., Prota, A., Schelling, P., Pilger, B., Folkers, G., Scapozza, L., and Schulz, G. E. (2000) *Proteins* **41,** 545–553
22. Sienaert, R., Naesens, L., Brancale, A., De Clercq, E., McGuigan, C., and Balzarini, J. (2002) *Mol. Pharmacol.* **61,** 249–254
23. Brown, D. G., Visse, R., Sandhu, G., Davies, A., Rizkallah, P. J., Melitz, C., Summers, W. C., and Sanderson, M. R. (1995) *Nat. Struct. Biol.* **2,** 876–881
24. Wild, K., Bohner, T., Aubry, A., Folkers, G., and Schulz, G. E. (1995) *FEBS Lett.* **368,** 289–292
25. Wild, K., Bohner, T., Folkers, G., and Schulz, G. E. (1997) *Protein Sci.* **6,** 2097–2106
26. Champness, J. N., Bennett, M. S., Wien, F., Visse, R., Summers, W. C., Herdewijn, P., de Clerq, E., Ostrowski, T., Jarvest, R. L., and Sanderson, M. R. (1998) *Proteins* **32,** 350–361
27. Otwinowski, Z., and Minor, W. (1996) *Methods Enzymol.* **276,** 307–326
28. Brunger, A. T., Adams, P. D., Clore, G. M., Delano, W. L., Gros, P., Grosse, K. R. W., Jiang, J. S., Kuszewski, J., Nilges, M., Pannu, N. S., Read, R. J., Rice, L. M., Simonson, T., and Warren, G. L.(1998) *Acta Crystallogr. Sec. D* **54,** 905–921

29. Prota, A., Vogt, J., Pilger, B., Perozzo, R., Wurth, C., Marquez, V. E., Russ, P., Schulz, G. E., Folkers, G., and Scapozza, L. (2000) *Biochemistry* **39,** 9597–9603
30. Schulz, G. E., and Schirmer, R. H. (1974) *Nature* **250,** 142–144
31. Dreusicke, D., Karplus, P. A., and Schulz, G. E. (1988) *J. Mol. Biol.* **199,** 359–371
32. Honess, R. W., Craxton, M. A., Williams, L., and Gompels, U. A. (1989) *J. Gen. Virol.* **70,** 3003–3013
33. Griffin, A. M., and Boursnell, M. E. (1990) *J. Gen. Virol.* **71,** 841–850
34. Balasubramaniam, N. K., Veerisetty, V., and Gentry, G. A. (1990) *J. Gen. Virol.* **71,** 2979–2987
35. Sulpizi, M., Schelling, P., Folkers, G., Carloni, P., and Scapozza, L. (2001) *J. Biol. Chem.* **276,** 21692–21697
36. Alber, F., Kuonen, O., Scapozza, L., Folkers, G., and Carloni, P. (1998) *Proteins* **31,** 453–459
37. Jones, G., Willett, P., Glen, R. C., Leach, A. R., and Taylor, R. (1997) *J. Mol. Biol.* **267,** 727–748
38. Kalé, L., Skeel, R., Bhandarkar, M., Brunner, R., Gursoy, A., Krawetz, N., Phillips, J., Shinozaki, A., Varadarajan, K., and Schulten, K. (1999) *J. Comput. Phys.* **151,** 283–312
39. McGuigan, C., Yarnold, C. J., Jones, G., Velazquez, S., Barucki, H., Brancale, A., Andrei, G., Snoeck, R., De Clercq, E., and Balzarini, J. (1999) *J. Med. Chem.* **42,** 4479–4484
40. Balzarini, J., and McGuigan, C. (2002) *J. Antimicrob. Chemother.* **50,** 5–9
41. Bennett, M. S., Wien, F., Champness, J. N., Batuwangala, T., Rutherford, T., Summers, W. C., Sun, H., Wright, G., and Sanderson, M. R. (1999) *FEBS Lett.* **443,** 121–125
42. De Clercq, E., Andrei, G., Snoeck, R., De Bolle, L., Naesens, L., Degreve, B., Balzarini, J., Zhang, Y., Schols, D., Leyssen, P., Ying, C., and Neyts, J. (2001) *Nucleosides Nucleotides and Nucleic Acids* **20,** 271–285